A Multiscale Simulation of Polymer Processing Using Parameter-Based Bridging in Melt Rheology

Yuichi Masubuchi,[1] Takashi Uneyama,[1,2] Keiichi Saito[3]

[1]*Institute for Chemical Research, Kyoto University, Gokasho, Uji 611-0011, Japan*
[2]*CREST, Japan Science and Technology Agency, Kawaguchi 332-0012, Japan*
[3]*Cybernet Systems Co. Ltd., Kanda-neribeicho, Chiyoda-ku, Tokyo 101-0022, Japan*

Received 22 March 2011; accepted 28 November 2011
DOI 10.1002/app.36593
Published online 30 January 2012 in Wiley Online Library (wileyonlinelibrary.com).

ABSTRACT: To investigate the effect of molecular structure on macroscopic flow behavior of polymeric liquid, attempts have been made to embed the microscopic information into the flow simulation. Constitutive equation based on the theory of polymer dynamics is ideal but the theory is still under development. The CONNFFESSIT approach (where microscopic simulation is embedded into calculation grid in macroscopic simulation) is another promising direction but the computational cost is not practical yet. In this study, we propose another simple method using parameter-based bridging where the parameters for phenomenological constitutive equations in macroscopic flow simulation are obtained from coarse-grained molecular simulation. As an example, we performed a simulation of injection molding and examined the effect of molecular weight on warpage of the molded product. We used the primitive chain network simulation to calculate linear viscoelasticity of linear monodispersed polystyrenes from molecular weight. The obtained linear viscoelasticity was converted into the relaxation spectrum and into the flow curve to be used in the macroscopic simulations. From the flow curve, the parameters of an inelastic non-Newtonian constitutive equation were obtained and used for the simulation of filling process. The relaxation spectrum was used to calculate residual stress from the flow profile in the filling process. From the residual stress and thermal shrinkage, warpage of the product was obtained. For the examined thin plate product, significant change in the warpage direction was demonstrated according to the molecular weight of the material. © 2012 Wiley Periodicals, Inc. J Appl Polym Sci 125: 2740–2747, 2012

Key words: simulations; rheology; injection molding; computer modeling

INTRODUCTION

It has been reported that the molecular architecture affects processability of polymeric materials.[1] For example, injection-molded products show warpage (which is anisotropic shrinkage) dependently on the processing conditions. One of the dominant mechanisms of the warpage is the molecular orientation induced by the competition between deformation and relaxation of the polymers during the process.[2] Because the molecular relaxation is dominated by the molecular architecture such as molecular weight and long-chain branching,[3] the warpage is affected by the molecular architecture.

Although it is demanded to predict the effect of molecular architecture on polymer processing, it is difficult to realize such a calculation by a single-simulation scheme. For instance, molecular simulation is ideal in general to investigate the effect of molecular architecture. However, for polymeric materials, the calculation cost is impractical because the relaxation time of polymers is much larger than the timescale realized by the molecular simulation. The length scale of interest in polymer processing is tremendously larger than the molecular scale as well. On the other hand, fluid dynamics simulation is useful for processing simulations but the molecular characteristic is not explicitly taken account in general.

Thus, there have been attempts on so-called multiscale or multidiscipline simulation that is combination of a couple of different simulations. The basic idea of multiscale simulation for polymeric materials has been rather established from the quantum scale to the mechanical scale containing several intermediate length (and time) scales.[4] Several simulations have been developed for each length scale based on different models, and the methods and theories have been proposed to bridge different simulations.

For polymer processing, in particular, the bridging (between molecular architecture and processing phenomena) has been made by constitutive equation that reflects the molecular architecture through rheology. Indeed, the development of molecular constitutive equation has been a major topic in polymer rheology[5] and flow simulations with constitutive equations (such as the pom–pom model,[6,7] the Rolie-Poly model,[8,9] and the Iannirruberto-Marrucci

Correspondence to: Y. Masubuchi (mas@scl.kyoto-u.ac.jp).

model[10]) have been made for complex flow geometries. For instance, Bent et al.[11] reported molecular stretch in a contraction–expansion flow geometry with the Rolie-Poly equation. Hassell et al.[12] further reported the molecular mechanism of flow instabilities. Wapperom and Keunings have reported flow calculations in similar contraction–expansion geometry to report the effect of convective constraint release in the Iannirruberto-Marrucci model[13] and the effect of long-chain branching in the pom–pom model.[14]

Another idea for the bridging is so-called CONNFFESSIT[15] where the polymer contribution in Eulerian fluid dynamics simulation is obtained from stochastic molecular simulation instead of the constitutive equation.[16,17] Several developments have been inspired by the CONNFFESSIT. For example, the configuration field method[18] has been developed and applied to the Doi-Edwards model in a complex flow.[19] Murashima and Taniguchi[20] have reported the direct embedding of a slip-link simulation to a Lagrangian fluid dynamics simulation.

Apart from the abovementioned approaches, another possible idea for the bridging is parameter-based approach where parameters for macroscopic simulation are obtained from microscopic simulation. This approach has been used in the bridging between atomistic and coarse-grained molecular simulations. For example, parameters for interaction potentials of the coarse-grained simulation are determined to reproduce the structural statistics in the atomistic simulations.[4,21] Recent developments have been made to extract the parameters for tube models from atomistic simulations.[22–24]

The parameter-based bridging is rather easy to be realized in any combination of simulations because the coupling between simulations is weak. For simulation of polymer processing, the parameter-based idea is also applicable to perform flow simulations with empirical constitutive equations if the parameters are obtained from molecular simulations. Although the idea seems straightforward, such an attempt has never been reported to the best of our knowledge.

In this article, we demonstrate the parameter-based bridging in polymer processing simulations on the effect of molecular weight on warpage of injection-molded product. The flow simulations are performed with a commercial software package, where the empirical constitutive equations are used. The parameters of the constitutive equations are usually obtained from experimental data but we obtained these parameters from a molecular simulation. Because the required time scale to obtain the parameters is significantly larger than the available time range for atomistic simulations and even for coarse-grained molecular simulations,[25,26] we use the primitive chain network (PCN) simulation[27] where the dynamics of entanglement segment is calculated.

The effect of processing conditions on warpage has been investigated (both with experiments and simulations) to report the effective factors, i.e., filling time, mold temperature, gate dimensions, melt temperature, packing pressure, packing time, etc.,[28–30] and it has been discussed that some of the processing conditions are dominant for warpage through residual stress induced by the molecular orientation.[1,2,28–30] However, the effect of molecular weight has never been examined. Because experimental approach is not practical due to the required amount of material, the position of this study is to propose a possible approach with simulations.

MODEL AND SIMULATIONS

Data-flow in the multiscale simulation

Figure 1 shows a schematic diagram of the data-flow in the parameter-based multiscale simulation proposed in this study. The viscoelasticity of the material is predicted with the PCN simulations for different molecular weights. The obtained rheological behavior is cast into the phenomenological constitutive equations to perform the flow simulation of the filling process. From the resultant profile of temperature and flow, residual stress distribution was obtained. Finally, by the obtained distributions of temperature and residual stress, warpage of the molded product was calculated. Detail of each calculation is given below.

PCN simulations

PCN model[27] is a multichain sliplink model where the entangled polymers are represented by consecutive segments. The representing molecular weight of the segment roughly corresponds to 60% of the entanglement molecular weight.[30,31] Each segment is bundled with another segment (that mostly belongs to another chain) via sliplink representing entanglement. Dynamics of the system is described by the motion of the sliplinks, the monomer transportation (chain slippage) though the sliplinks, and creation and destruction of the sliplinks. Thus, the state variables are position of the sliplinks $\{\mathbf{R}\}$, the number of monomers on each segment $\{n\}$, and the number of sliplinks on each polymer $\{Z\}$. The kinetic equation for $\{\mathbf{R}\}$ and $\{n\}$ is written as

$$2\zeta \frac{d\mathbf{R}}{dt} = \frac{3kTn_0}{a^2} \sum_j^4 \frac{\mathbf{r}_j}{n_j} + 2n_0 \nabla \mu + \mathbf{F}^r \tag{1}$$

$$\frac{\zeta}{\varphi} \frac{dn}{dt} = \frac{3kTn_0}{a^2} \left(\frac{r_{i+1}}{n_{i+1}} - \frac{r_i}{n_i} \right) + n_0 \nabla \mu + f^r \tag{2}$$

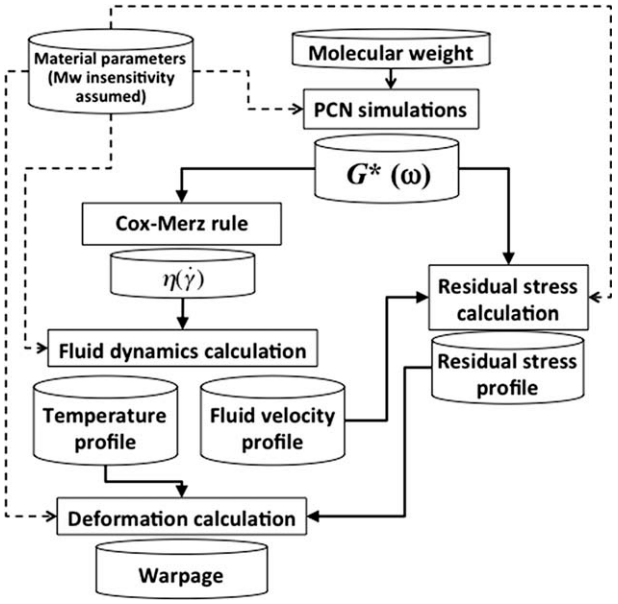

Figure 1 Schematic diagram of data flow.

Equation (1) is the Langevin type equation of motion for {**R**} and the left-hand side is the drag force, and ζ is the friction coefficient of the segment (thus, 2ζ is the friction of one sliplink bundling two segments). The first term in the right-hand side is the tension balance around the sliplink among four conversing segments to the sliplink, a is the average length of the segment under equilibrium, **r** is the segment bond vector, n is the monomer number on the segment, and n_0 is the average under equilibrium of n. The second term in the right-hand side of eq. (1) is the osmotic force generated by density fluctuation of the network, and μ is the chemical potential derived from the local free energy given by

$$A = \begin{cases} \kappa \left(\frac{\phi(\mathbf{R})}{\langle \phi \rangle} - 1 \right)^2 & \text{for} \quad \phi(\mathbf{R}) > \langle \phi \rangle \\ 0 & \text{for} \quad \phi(\mathbf{R}) \leq \langle \phi \rangle \end{cases} \tag{3}$$

Here, κ is a phenomenological parameter to avoid clustering of sliplinks and $\phi(\mathbf{R})$ is the number density of sliplink and $\langle \phi \rangle$ is the average of $\phi(\mathbf{R})$ under equilibrium for the overall system. κ and $\langle \phi \rangle$ are fixed at 0.5 and 10, respectively, in this particular study. The third term in the right-hand side of eq. (1) is the random force obeying $\langle \mathbf{F}^r \rangle = \mathbf{0}$ and $\langle \mathbf{F}^r{}_i(t) \cdot \mathbf{F}^r{}_j(t') \rangle = 12kT\zeta\delta_{ij}\,\delta(t - t')$.

Equation (2) is the rate-change equation for $\{n\}$ and the driving forces are common to eq. (1) but the force balance is described in one-dimension (along the chain). φ in the left-hand side is the local segment density given by

$$\varphi = \frac{1}{2}\left(\frac{n_{i+1}}{r_{i+1}} + \frac{n_i}{r_i} \right) \tag{4}$$

r in the first term in the right-hand side of eq. (2) is the segment length. f^r in the third term is the random force in one-dimension obeying $\langle f^r \rangle = 0$ and $\langle f^r{}_i(t) \cdot \mathbf{f}^r{}_j(t') \rangle = 2kT\zeta\delta_{ij}\,\delta(t - t')$. Note that eqs. (1) and (2) are coupled via r and n.

The time development of {Z} is realized by the creation and destruction of sliplinks at chain ends. The destruction of sliplink occurs when the monomer number at the end segment becomes less than a certain critical value. On the contrary, when the monomer number exceeds another critical value, a new sliplink is created at the tested end segment with hooking another segment chosen randomly from surrounding segments. The used monomer number window is

$$0.5 < n/n_0 < 1.5 \tag{5}$$

The stress tensor is calculated from the trajectory by

$$\sigma = 3G_0\left\langle \frac{\mathbf{rr}}{n} \right\rangle \tag{6}$$

Here, G_0 is the unit modulus.

The simulations were performed with nondimensional equations where we chose a as unit length, kT as unit energy, and $\zeta a^2/6kT$ as unit time (τ_0). The simulations were performed with the periodic boundary condition with the cell dimension of 12^3. The effect of wall (mold) is not taken account because only the bulk property is required in this study. The parameters are chosen to reproduce polystyrene melts where unit of molecular weight M_0 ($= M/Z$) is 11 k, G_0 is 0.33 MPa and $\tau_0 = 2$ m s for $T = 453$ K. τ_0 for the other temperatures are given by the Williams-Landel-Ferry (WLF) relationship.[3] Although PCN simulation can be used for various systems with branching structure and with molecular weight distribution,[32–35] in this particular study, the simulations were restricted to linear monodispersed melts only. In this respect, the other sliplink simulations[36–38] and the molecular-based constitutive equations (mentioned in the previous section for example) are also applicable to this particular study.

Macroscopic simulations

The flow analysis in the filling process was performed under the Hele-Shaw flow assumption.[39,40] The governing equations standing for the conservation of mass, momentum, and energy are

$$\frac{\partial \rho}{\partial t} + \frac{\partial}{\partial x}\left(\int dz \rho u \right) + \frac{\partial}{\partial x}\left(\int dz \rho v \right) = 0 \tag{7}$$

$$\frac{\partial p}{\partial x} = \frac{\partial \sigma_{zx}}{\partial z}, \quad \frac{\partial p}{\partial y} = \frac{\partial \sigma_{zy}}{\partial z} \tag{8}$$

$$\rho C_p \left(\frac{\partial T}{\partial t} + u \frac{\partial T}{\partial x} + v \frac{\partial T}{\partial y} \right) = \frac{\partial}{\partial z} \left(\lambda_z \frac{\partial T}{\partial z} \right) + \sigma_{zx} \frac{\partial u}{\partial z} + \sigma_{yz} \frac{\partial v}{\partial z} \quad (9)$$

Here, ρ is the density, u and v are the fluid velocity in x direction [machine direction (MD)] and y direction [transverse direction (TD)], respectively, and p is the pressure. C_p is the heat capacity and λ_z is the thermal conductivity. σ is the stress tensor. u and v satisfy the nonslip boundary condition on the wall. We notice that, in eq. (9), we have assumed that the density gradient is much smaller than the velocity and temperature gradients.

For the constitutive equation to obtain the stress tensor, an inelastic non-Newtonian equation is used with the WLF-type temperature dependence.

$$\sigma_{zx} = \eta \frac{\partial u}{\partial z}, \quad \sigma_{yz} = \eta \frac{\partial v}{\partial z} \quad (10)$$

$$\eta(\dot{\gamma}, T) = \frac{\eta_T(T)}{1 + C_1(\eta_T(T)\dot{\gamma})^{C_2}}, \quad \eta_T(T) = C_3 \exp\left(-\frac{C_4(T - T_r)}{C_5 + T - T_r} \right) \quad (11)$$

Here $\{C_1, \ldots, C_5\}$ are the material parameters and T_r is the reference temperature. $\dot{\gamma}$ is the component of the shear rate tensor.

For the state equation, Spencer-Gilmore equation[41] is used.

$$(p + \hat{p}) \left(\frac{1}{\rho} - \frac{1}{\hat{\rho}} \right) = \hat{R}T \quad (12)$$

Here, $\hat{p}$, $\hat{\rho}$, and $\hat{R}$ are the material parameters and the change of these parameters at T_g is taken account as shown later. At the injection front, we impose the constant pressure condition.

$$p = p_0 \quad \text{(at the injection front)} \quad (13)$$

where p_0 is the atmospheric pressure.

After the filling process, the cooling process was calculated to obtain temperature distribution. Then from the obtained thermal and flow history, according to the method proposed by Baaijens,[42] the residual stress was calculated with the multimode Leonov constitutive equation[43]

$$\sigma' = 2\eta_0 \mathbf{g} + \sum_{k=1}^{N} \mu_k \mathbf{C}_k \quad (14)$$

$$\frac{\partial \mathbf{C}_k}{\partial t} + (\varpi + \mathbf{g}) \cdot \mathbf{C}_k - \mathbf{C}_k \cdot (\varpi + \mathbf{g}) + \frac{1}{6\theta_k} \left[3\mathbf{C}_k^2 - \left(\mathrm{tr}\mathbf{C}_k - \mathrm{tr}\mathbf{C}_k^{-1} \right) \mathbf{C}_k - 3\mathbf{I} \right] = 0 \quad (15)$$

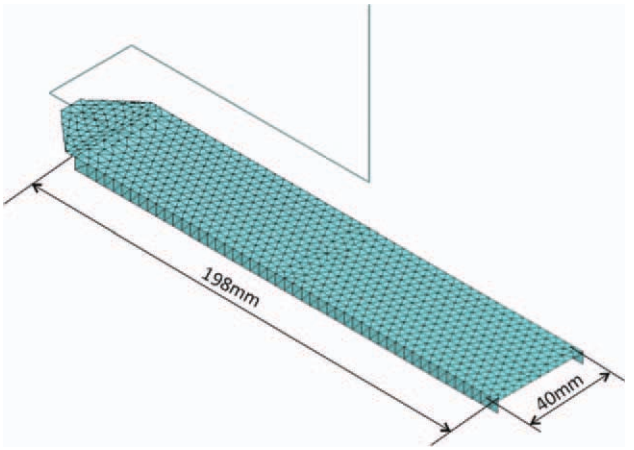

Figure 2 Model for the macroscopic calculations. [Color figure can be viewed in the online issue, which is available at wileyonlinelibrary.com.]

Here, σ' is the residual stress tensor, η_0 is the effective Newtonian viscosity, and $\mathbf{g}$ is the shear rate tensor. μ_k, $\mathbf{C}_k$, and θ_k are the relaxation intensity, the Finger strain tensor, and the relaxation time of the kth mode, respectively. $\varpi + \mathbf{g}$ and $\mathbf{I}$ are the rate of rotation tensor and the unit tensor, respectively. ($\varpi + \mathbf{g}$ corresponds to the velocity gradient tensor.)

According to the residual stress profile and the temperature profile, local strain tensor ε is calculated for warpage by the following set of equations.

$$\begin{bmatrix} \varepsilon_{xx} \\ \varepsilon_{yy} \\ \varepsilon_{xy} \end{bmatrix} = (T - T_R) \begin{bmatrix} \alpha_{xx} & 0 & 0 \\ 0 & \alpha_{yy} & 0 \\ 0 & 0 & 0 \end{bmatrix} \begin{bmatrix} 1/2 \\ 1/2 \\ 0 \end{bmatrix} + \mathbf{D}^{-1} \cdot \begin{bmatrix} \sigma'_{xx} \\ \sigma'_{yy} \\ \sigma'_{xy} \end{bmatrix} \quad (16)$$

$$\mathbf{D} = \frac{E}{1 - \nu^2} \begin{bmatrix} 1 & \nu & 0 \\ \nu & 1 & 0 \\ 0 & 0 & 1 - \nu \end{bmatrix} \quad (17)$$

Here, α_{xx} and α_{yy} are the thermal expansion coefficient in MD and TD direction (shown later in Fig. 3), T_R is the room temperature (the observed temperature for warpage), E is the Young's modulus, and ν is the Poisson's ratio.

The flow simulations were performed for a two layered shell model, which has 872 nodal points and 1565 triangular elements (see Fig. 2) to represent a plate shape product with side ribs. The temperature of the upper and lower molds and the melt polymers at the injection are fixed at 20°C, 40°C, and 200°C, respectively. The filling time and packing time were 1 s and 3 s, respectively. The packing pressure was 4903 Pa (500 kgf cm^{-2}).

In this study, we assume that the material parameters are dependent on molecular weight for rheology only, and the parameters to describe rheology were obtained from PCN simulations. (The values

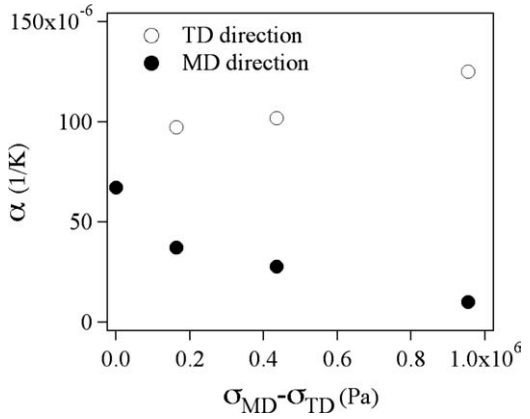

Figure 3 Used thermal expansion coefficients dependent on normal stress and flow direction.

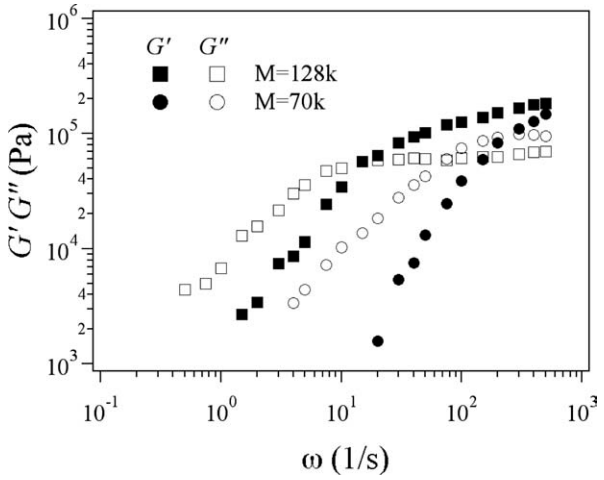

Figure 4 Linear viscoelasticity of polystyrene melts calculated by primitive chain network simulations.

will be presented in the next section.) The rest of the parameters are independent of molecular weight and fixed as $C_v = 1.70$ kJ kg^{-1} K^{-1}, $\lambda_z = 0.12$ W m^{-1} K^{-1}, $C_4 = 12.00$, $C_5 = 1.241 \times 10^2$ K, and $T_r = 453$ K. $\hat{p}$, $\hat{\rho}$, and $\hat{R}$ in eq. (12) are 1.079×10^8 Pa, 1.185×10^3 kg m^{-3}, and 42.86 J kg^{-1} K^{-1} for $T < T_c$, otherwise 1.966×10^8 Pa, 1.321×10^3 kg m^{-3}, and 12.45 J kg^{-1} K^{-1}. The critical temperature T_c depends on pressure expressed as

$$T_c = \frac{C_6}{p} + C_7 \tag{18}$$

Here, C_6 and C_7 are fixed at $C_6 = 2.547 \times 10^{-7}$ K Pa^{-1} and $C_7 = 365.7$ K. In eq. (16), the thermal expansion coefficient is anisotropic[44] due to the molecular stretch and it is shown in Figure 3, where the thermal expansion coefficient is differently expressed for TD and MD directions as functions of the normal stress difference. In eq. (17), $\nu = 0.38$ and $E = 2.32$ GPa.

The macroscopic calculations were performed with a commercially available solver (PLANETS MoldStudio, Cybernet Co.), and the parameters shown above were provided in the material database in the used software package.

RESULTS AND DISCUSSION

Figure 4 shows the linear viscoelasticity of the polystyrene melts with two different molecular weight of $M = 70$ k and 128 k. It has been reported that those data are quantitatively in good agreement with experiments.[45] From these data, the parameters for macroscopic calculations were obtained as summarized in Table I. The viscoelastic spectrum for eq. (14) was obtained from these data. The parameters $C_1 - C_3$ in eq. (11) were also obtained from the linear viscoelastic response with the Cox-Merz rule. We note that $C_1 - C_3$ can be directly obtained from PCN simulations under flow[46] but in this particular study those parameters were obtained from the linear viscoelastic response for convenience and noise-reduction purpose. Note that due to the model restriction glassy behavior cannot be predicted, and thus, it is not taken account of in the fitting.

Figure 5 shows the residual stress distribution after the filling. Because of the flow into the ribs located in both side, deformation rate becomes higher in the top plane than that in the bottom plane, and thus, the higher residual stress is observed in the top plane. The higher residual stress is also contributed by the slower relaxation of the top area, which is according to the lower temperature of the top plane. Concerning the molecular weight, the longer molecule ($M = 128$ k) generates the larger residual stress, reflecting the difference in relaxation spectrum, i.e., the longer molecule has relaxation modes with long-relaxation times (see Table I) and those modes do not relax in the filling and packing processes. Note that the obtained residual stress is generated by rubbery and terminal relaxation modes, and the glassy modes are neglected as mentioned above. We believe that the

TABLE I
Material Parameters at 453 K Obtained from the Data in Figure 4

	$M = 70$ k	$M = 128$ k
C_1	3.40×10^{-7}	1.24×10^{-6}
C_2	1.00	0.95
C_3 (Pa s)	9.97×10^2	8.74×10^3
μ_1 (Pa)	8.33×10^4	4.00×10^5
μ_2 (Pa)	–	4.87×10^4
μ_3 (Pa)	–	2.87×10^3
θ_1 (s)	5.07×10^{-3}	6.78×10^{-3}
θ_2 (s)	–	6.21×10^{-2}
θ_3 (s)	–	3.64×10^{-1}

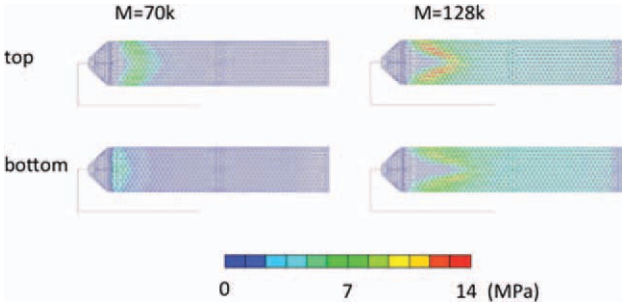

Figure 5 Residual stress profiles. Colors indicate the absolute value in the normal direction. [Color figure can be viewed in the online issue, which is available at wileyonlinelibrary.com.]

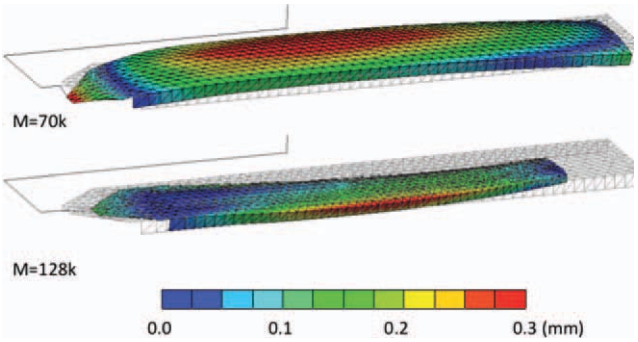

Figure 7 Final shape of the product. Colors indicate absolute value of normal displacement from the initial position. [Color figure can be viewed in the online issue, which is available at wileyonlinelibrary.com.]

glassy modes do not have significant effect on the observed difference for the molecular weight because the glassy modes relax during the filling process. It is also noted that the decomposition of the residual stress into molecular stretch and orientation is not possible because the molecular detail is lost in the continuum simulation (due to the use of phenomenological constitutive equations).

Figure 6 shows the temperature distribution after the filling. According to the setup, temperature in the upper plane is higher than that in the lower plane (note that the upper and the lower mold is at 20°C and 40°C, respectively). Thus, there exists a contribution of thermal deformation generated by this temperature difference between top and bottom planes, and the contribution is somewhat larger for $M = 70$ k because the temperature difference is relatively small for $M = 128$ k due to the heat generated by its higher viscosity.

Figures 7 and 8 show the warpage resulted by the competition between the thermal deformation and the residual stress. To observe the warpage, rotation and translation of the plate are eliminated. For $M =$ 70k, the dominant mechanism of warpage is the thermal deformation generated by the difference in the mold temperature (see Fig. 6) so that a convex shape is realized reflecting the larger expansion for the higher temperature. On the contrary, for $M =$ 128k, deformation originated by the residual stress is dominant, and thus, a concave shape is observed according to the difference of the residual stress between top and bottom planes as shown in Figure 5.

Because the larger residual stress for longer molecule is generated by the longer relaxation time, from the viewpoint of the Deborah number (which is the product of deformation rate and relaxation time), the observed effect of molecular weight may be converted into that of the processing conditions for temperature and deformation rate, e.g., melt temperature, filling time, etc. For instance, Huang and Tai[28] investigated the effective factors for warpage to report that the melt temperature is comparably influential to the packing pressure and the mold temperature. This is consistent with our result but the contributions from the thermal deformation and the residual stress cannot be separated through the

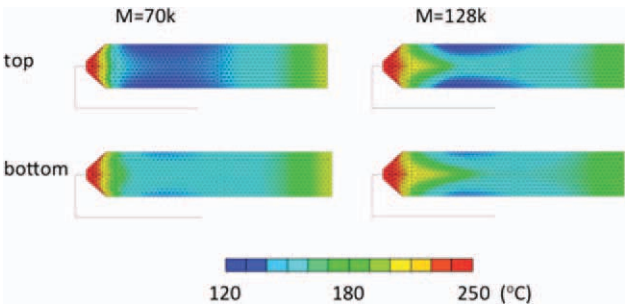

Figure 6 Temperature distributions. [Color figure can be viewed in the online issue, which is available at wileyonlinelibrary.com.]

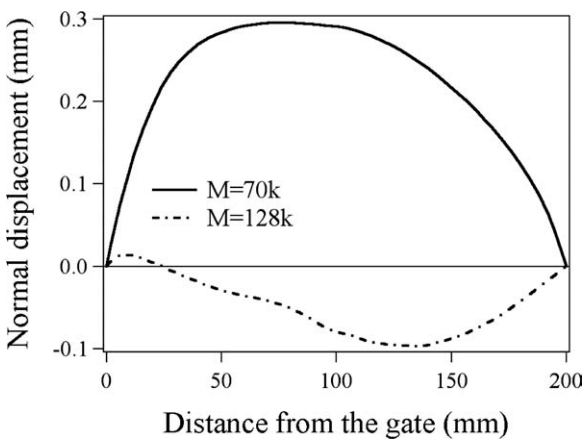

Figure 8 Normal displacement of the product in the machine direction along the central line from the gate.

analysis on the melt temperature. In this respect, experimental validation of the presented result is required. We postpone it as a future work because it is beyond the scope of this study where we propose the multiscale simulation for polymer processing using the parameter bridging.

CONCLUSIONS

A simple scheme of multiscale simulation is proposed to investigate the effect of molecular structure on the polymer processing. The coupling between molecular simulation and continuum calculation was realized by parameter-based bridging where the parameters for macroscopic calculation were obtained from molecular simulation. As an example, the effect of molecular weight on warpage of an injection-molded product was demonstrated. The PCN simulation is used to calculate linear viscoelasticity of linear monodispersed polystyrenes from molecular weight. The linear viscoelasticity was converted to the relaxation spectrum and the flow curve and used in the macroscopic simulations. From the flow curve, the parameters of an inelastic non-Newtonian constitutive equation were obtained and used for simulation of the filling process. The relaxation spectrum was used to calculate residual stress from the flow profile. From the residual stress and thermal shrinkage, warpage of the product was obtained. For the examined thin plate product, significant change in the warpage direction was demonstrated according to the molecular weight. The advantage of the proposed approach is the weak coupling between simulations, which does not affect calculation cost and does not cause any numerical difficulties in each simulation. Further notice is made in comparison with the CONNFFESSIT type approach on the noise reduction. In the proposed approach, the noise generated in microscopic simulation does not propagate to macroscopic simulation because output of the microscopic simulation is not directly given to the macroscopic simulation but the result of microscopic simulation is converted into macroscopic constitutive equations. Although the microscopic information is abandoned, it is possible to reconstruct it via additional microscopic calculations along the obtained trace of the flow element, for example. Studies in this direction have been performed and the results will be published elsewhere.

The authors thank A. Hayashigaki, Y. Nakahara, A. Watanabe, and K. Tada in Cybernet Co. for their help on the use of PLANETS software.

References

1. Tadmor, Z.; Gogos, C. G. Principles of Polymer Processing, 2nd ed.; Wiley: Hoboken, 2006.
2. Tadmor, Z. J Appl Polym Sci 1974, 18, 1753.
3. Ferry, J. D. Viscoelastic Properties of Polymers, 3rd ed.; Wiley: New York, 1980.
4. Müller-Plathe, F. Chem Phys Chem 2002, 3, 754.
5. Doi, M.; Edwards, S. F. The Theory of Polymer Dynamics; Clarendon: Oxford, 1986.
6. McLeish, T. C. B.; Larson, R. G. J Rheol 1998, 42, 81.
7. Verbeeten, W. M. H.; Peters, G. W. M.; Baaijens, F. P. T. J Rheol 2001, 45, 823.
8. Graham, R. S.; Likhtman, A. E.; McLeish, T. C. B.; Milner, S. T. J Rheol 2003, 47, 1171.
9. Likhtman, A. E.; Graham, R. S. J Non-Newtonian Fluid Mech 2003, 114, 1.
10. Ianniruberto, G.; Marrucci, G. J Rheol 2001, 45, 1305.
11. Bent, J.; Hutchings, L. R.; Richards, R. W.; Gough, T.; Spares, R.; Coates, P. D.; Grillo, I.; Harlen, O. G.; Read, D. J.; Graham, R. S.; Likhtman, A. E.; Groves, D. J.; Nicholson, T. M.; McLeish, T. C. B. Science 2003, 301, 1691.
12. Hassell, D. G.; Mackley, M. R.; Sahin, M.; Wilson, H. J.; Harlen, O. G.; McLeish, T. C. B. Phys Rev E 2008, 77, 050801–1.
13. Wapperom, P.; Keunings, R. J Non-Newtonian Fluid Mech 2000, 95, 67.
14. Wapperom, P.; Keunings, R. J Non-Newtonian Fluid Mech 2001, 97, 267.
15. Laso, M.; Öttinger, H. C. J Non-Newtonian Fluid Mech 1993, 47, 1.
16. Öttinger, H. C.; Laso, M. In Lectures on Thermodynamics and Statistical Mechanics: Proceedings of the XXII Winter Meeting on Statistical Physics; López de Haro, M., Varea, C., Eds.; World Scientific: Singapore, 1994.
17. Hua, C. C.; Schieber, J. D. J Rheol 1998, 42, 477.
18. Hulsen, M. A.; van Heel, A. P. G.; van den Brule, B. H. A. A. J Non-Newtonian Fluid Mech 1997, 70, 79.
19. van Heel, A. P. G.; Hulsen, M. A.; van den Brule, B. H. A. A. J Rheol 1999, 43, 1239.
20. Murashima, T.; Taniguchi, T. J Polym Sci Part B: Polym Phys 2010, 48, 886.
21. Guenza, M. G. J Phys Condens Matter 2008, 20, 033101–1.
22. Tzoumanekas, C.; Theodorou, D. N. Curr Opin Solid State Mater Sci 2006, 10, 61.
23. Stephanou, P. S.; Baig, C.; Tsolou, G.; Mavrantzas, V. G.; Kroger, M. J Chem Phys 2010, 132, 124904–1.
24. Sukumaran, S. K.; Likhtman, A. E. Macromolecules 2009, 42, 4300.
25. Kremer, K.; Grest, G. S. J Chem Phys 1990, 92, 5057.
26. Likhtman, A. E.; Sukumaran, S. K.; Ramirez, J. Macromolecules 2007, 40, 6748.
27. Masubuchi, Y.; Takimoto, J.-I.; Koyama, K.; Ianniruberto, G.; Marrucci, G.; Greco, F. J Chem Phys 2001, 115, 4387.
28. Huang, M.-C.; Tai, C.-C. J Mater Process Technol 2001, 110, 1.
29. Zoetelief, W. F.; Douven, L. F. A.; Ingen housz, A. J. Polym Eng Sci 1996, 36 1886.
30. Kabanemi, K. K.; Vaillancourt, H.; Wang, H.; Salloum, G. Polym Eng Sci 1998, 38, 21.
31. Masubuchi, Y.; Ianniruberto, G.; Greco, F.; Marrucci, G. J Chem Phys 2003, 119, 6925.
32. Masubuchi, Y.; Ianniruberto, G.; Greco, F.; Marrucci, G. Model Simul Mater Sci Eng 2004, 12, S91.
33. Masubuchi, Y.; Ianniruberto, G.; Greco, F.; Marrucci, G. J Non-Crystal Solids 2006, 352, 5001.
34. Masubuchi, Y.; Ianniruberto, G.; Greco, F.; Marrucci, G. Rheol Acta 2006, 46, 297.
35. Masubuchi, Y.; Watanabe, H.; Ianniruberto, G.; Greco, F.; Marrucci, G. Macromolecules 2008, 41, 8275.
36. Doi, M.; Takimoto, J.-I. Philos Trans R Soc London Ser A 2003, 361 641.

37. Likhtman, A. E. Macromolecules 2005, 38, 6128.
38. Nair, D. M.; Schieber, J. D. Macromolecules 2006, 39, 3386.
39. Hieber, C. A.; Shen, S. F. J Non-Newtonian Fluid Mech 1980, 7, 1.
40. Kamal, M. R.; Chu, E.; Lafleur, P. G.; Ryan, M. E. Polym Eng Sci 1986, 26, 190.
41. Spencer, R. S.; Gilmore, G. D. J Appl Phys 1950, 21, 523.
42. Baaijens, F. P. T. Rheol Acta 1991, 30, 284.
43. Leonov, A. I. Rheol Acta 1976, 15, 85.
44. Pottiger, M. T.; Coburn, J. C.; Edman, J. R. J Polym Sci Part B: Polym Phys 1994, 32 825.
45. Masubuchi, Y.; Ianniruberto, G.; Greco, F.; Marrucci, G. J Non-Newtonian Fluid Mech 2008, 149, 87.
46. Masubuchi, Y.; Furuichi, K.; Horio, K.; Uneyama, T.; Watanabe, H.; Ianniruberto, G.; Greco, F.; Marrucci, G. J Chem Phys 2009, 131 114906–1.